Computational Fluid Dynamics Blood Flow Simulation by Patient-Specific Modeling of Aortic and Coronary Outlet

Ji-Song Jong., Ji-Song Thak., Sung-Ri Kim*., Hyon-Chol Choe., Kuk-Chol Song

Faculty of Mechanical Science and Technology, Kim Chaek University of Technology, Kyogu-dong No.60, Yonggwang Street, Pyongyang 950003, Democratic People's Republic of Korea

***Corresponding Author**

DOI: https://dx.doi.org/10.51244/IJRSI.2025.1215PH000192

Received: 27 September 2025; Accepted: 04 October 2025; Published: 20 November 2025

ABSTRACT

We develop a cardiovascular flow simulation system that performs a flow simulation analysis in patient-specific cardiovascular system and a bypass grafts suggested by a surgeon. In this simulation system, the vessels that are not reflected in the three-dimensional (3D) model of the vessel are modeled by an electrical circuit analogous model, and the simulation is carried out by combining the computational fluid dynamics (CFD) analysis of the vessel 3D model and analysis of the electrical analogous circuit. In order to evaluate the accuracy of the results by this simulation system we analyzed blood flow in cardiovascular system by ANSYS Fluent 19.2. In this paper, we study a method of setting boundary conditions for analyzing blood flow by ANSYS Fluent 19.2. We extract the patient-specific blood pressure (BP) waveforms at the aortic and coronary outlets from the electrical circuit analogous models of blood vessels such as Windkessel model and lumped parameter model. The parameter values of the analogous models are optimized to approximate the measured patient-specific systolic and diastolic pressure. By setting these blood pressure waveforms as outlet boundary conditions, we perform a simulation analysis of three-dimensional vascular model by ANSYS Fluent 19.2 and compare the results such as blood flow rates and blood pressures with clinical measurements. The comparison showed that the relative error in systolic pressure was -3.94~4.42%, diastolic pressure was -2.71~4.43%, and cardiac output was -4.76~4.8%, which demonstrated the accuracy of our boundary modeling and simulation analysis results.

Keyword: blood flow, cardiovascular, boundary modeling, CFD analysis, analogous model, electrical analogous circuit

INTRODUCTION

Cardiovascular disease is a leading cause of death worldwide and a lot of researches for improvement of medical treatment methodology for it are progressed so actively that many successes are achieved with the development of medical science and technology. Especially a coronary artery bypass graft surgery forms bypass grafts from aorta to post-stenosed region of coronary artery in order to increase a flow rate of blood to the region. In the process of applying to clinical treatment, this surgery is admitted as the most effective surgical treatment methodology for patients with cardiovascular disease. But this treatment methodology is costly and the disease often recurs. Hence, it is very important to estimate the effect of bypass graft surgery and correctly predict circulation state of blood in cardiovascular system after surgery, for which computational fluid dynamics blood flow simulation method is widely used.

The important aspect of cardiovascular flow simulation is the modeling of blood flow and the modeling of boundary conditions. Accurate assessment and modeling of the cardiovascular circulation has a great impact on the accuracy of blood flow simulations, and many studies have been carried out by researchers. Blood flow in cardiovascular system can be considered as laminar flow because of the relatively low Reynolds number flow, compressible or incompressible flow, Newtonian or non-Newtonian fluid flow depending on characteristics such as blood density and viscosity. Politis et al. (2007) assumed that blood flow was three-dimensional, steady, laminar flow and Newtonian flow, and the vessel wall was nonelastic and impermeable, and analyzed haemodynamic parameters such as velocity, pressure loss, wall shear stress and flow rates at specific locations

such as anastomosis. Ko et al. (2007) assumed blood flow to be three-dimensional, steady, laminar, incompressible flow and analyzed it using the continuity equation and Navier-Stokes equation. Blood is assumed to be Newtonian fluid and its density as 1 000kg/m3 and dynamics viscosity as 0.003 5kg/m•s, respectively. Bertolotti et al. (1999), Zhu et al. (2015), and Kandail et al. (2018) considered that vessel walls were rigid and non-porous and blood was viscous, incompressible, Newtonian and homogeneous. Basing on these assumptions, the conservation equations for three-dimensional, steady, laminar flow were solved by using finite volume based CFD solver.

However, some studies considered the blood flow as turbulent, considering the pulsatility of the flow and the swirl at the bifurcation point. Jayendiran et al. (2018) assumed blood to be a Newtonian, incompressible medium and blood flow to be pulsatile, turbulent and fully developed. Owida et al. (2012) assumed blood to be a homogeneous, non-deformable, chemically inert Newtonian fluid, and its density to be independent of pressure changes but only dependent on temperature changes.

How to model the cardiovascular inlet and outlet boundaries has a significant impact on the results of three-dimensional simulation of blood flow, and extensive research has been conducted. Modeling of boundary conditions is essentially to model parts that are not reflected in the 3D model for simulation analysis, i.e., to reflect the variation of the properties in the parts omitted from the 3D model as boundary conditions. Kamangar et al. (2007, 2017) applied the velocity inlet boundary and pressure outlet boundary as the simplest modeling of boundary condition. Ko et al. (2007) set the inlet boundary condition as a uniform velocity distribution and the outlet as a fully developed condition and applied a non-slip condition for the vessel wall. Owida et al. (2012), Ballarin et al. (2017), and Zhu et al. (2015) specified blood flow measured by duplex ultrasonography as inlet boundary condition and a zero static pressure as outlet boundary condition. Bertolotti et al. (1999) set three-dimensional Poiseuille velocity profiles as the inlet boundary condition, the no-slip condition for the vessel wall and traction-free surfaces as outlet boundary. McGah et al. (2011) applied a time-dependent Womersley velocity profile to mimic the patient-specific flow rates. Jayendiran et al. (2018) specified pressure distribution as inlet boundary condition and pressure value as outlet boundary condition. Kandail et al. (2018) numerically simulated the Navier-Stokes equation by setting transient blood flow waveforms to the aortic inlet and coronary outlets and a transient pressure waveform to the aortic outlet. Shaik et al. (2008) and Wang et al. (2014) used the blood flow waveform with heartbeat as an inlet boundary condition to simulate the propagation of wave by heartbeat. Fayssal et al. (2018), Segalova et al. (2012), and Fan et al. (2016) set the blood pressure or blood flow waveform as inlet boundary condition and the flow resistance as outlet boundary condition and analyzed the blood pressure and flow rate distribution by using the three-dimensional finite volume method. Updegrove et al. (2017), Schiavazzi et al. (2016), Kim et al. (2009, 2010), Lan et al. (2018), Vignon-Clementel et al (2010), Seo et al. (2020), Zhang et al. (2014), and Mirramezani et al. (2019) modeled heart and vasculars omitted in the three-dimensional model of a cardiovascular system by parameters such as resistance (R), inertance (L) and compliance (C) to form an electrical circuit analogous model and carried out the simulation analysis about the coupling of electrical circuit analogous modeling equation and Navier-Stokes equation of the three-dimensional model of vessels. Sankaran et al. (2012) and Zhao et al. (2016) modeled the downstream vascular by using a lumped parameter model comprised of resistance, compliance, inertance and diode obtained from the patient-specific clinical data and analyzed flow rate and pressure of the three-dimensional model through the finite element analysis and reflected these results in lumped parameter model again. In the same way they carried out the simulation analysis repeatedly until the convergence condition was satisfied. Zambrano et al. (2017) developed computational models considering the stiffness of pulmonary artery and describing Windkessel type parameter model for each outlet branch. Aboelkassem et al. (2019) modeled the arterial inlet by Windkessel-Womersley (WK-W) coupled model and the coronary outlet by 6-element Windkessel (WK6) model to predict the pulsation of blood flow and described the significance in development of basic theory of cardiovascular mechanics and clinical practice.

It is also important for simulation of blood flow in cardiovascular system to guarantee accuracy and ensure rapidity of the simulation analysis. Up to now CFD analysis tools such as Fluent, ANSYS CFX, etc. or developed private analysis tools were used in simulation analysis. Hazer et al. (2006) carried out the transient simulation analysis of partial cardiovascular system with an inlet velocity waveform by using Fluent 6.2. Horner et al. (2016) carried out the steady simulation analysis of patient-specific vascular model with mean flow rate and mean pressure as boundary conditions. Updegrove et al. (2017) and Lan et al. (2018) developed a fully open-

ISSN No. 2321-2705 | DOI: 10.51244/IJRSI | Volume XII Issue XV October 2025 | Special Issue on Public Health

source SimVascular software package, which was a private tool for the cardiovascular blood flow simulation analysis. In this package they carry out the transient analysis by using parameter models as boundary conditions.

Now we are developing a new simulation analysis system to simulate cardiovascular blood flow by building a patient-specific three-dimensional vascular model and modeling boundary conditions by parameters. And we regard CFD simulation analysis results and clinical measurements as comparative data to verify the accuracy of simulation analysis results from this simulation system. In order to compare simulation results from our developing simulation system with CFD simulation analysis results, boundary conditions must be the same. This simulation system models boundary conditions by parameters such as resistance (R), inertance (L) and compliance (C). To use these boundary models in simulation analysis by ANSYS Fluent 19.2, we extracted blood pressure waveforms from these analogue circuit models.

In this paper, we suggest the method to extract the patient-specific blood pressure waveforms from analogue circuit models of cardiovascular downstream by parameters and analyze blood flow by ANSYS Fluent 19.2 with these blood pressure waveforms.

MATERIALS AND METHODS

Three-dimensional geometric model

A three-dimensional geometry of the cardiovascular system is shown in Fig. 1.

This anatomy is constructed from computed tomography (CT) images by using our simulation system, is similar to patient-specific blood vessels and can be also used in analysis by ANSYS Fluent. The model consists of a segment of aortic arch and right and left coronary arteries. And blood flows into the aorto-coronary model through the aortic inlet and flows out from the aorto-coronary model through the aortic outlet and 5 right coronary artery (RCA) outlets and 6 left coronary artery (LCA) outlets. As can be seen in the figure, there are symmetric stenosis of 99% area-reduction and 5 mm length in middle and distal of the third segment of right coronary artery, respectively, and non-symmetric stenosis of 50% area-reduction and 4mm length in proximal of the fifth segment of main left coronary artery and non-symmetric stenosis of 70% area-reduction and 18mm length in proximal of the eleventh segment of left circumflex artery. We created a tetrahedral mesh of this model, in particular, implemented adapted mesh of stenoses with narrow diameters to ensure the accuracy of the simulation analysis.

Boundary conditions

Boundary conditions must be applied to the aortic inlet, outlet and coronary outlet in order to carry out CFD anaysis of this model. Blood flow waveform obtained by cardiac ultrasonography is used as flow rate boundary condition at the aortic inlet and blood pressure waveforms obtained from electrical circuit analogous models of downstream vasculars are utilized as pressure boundary conditions at the aortic outlet and coronary outlets.

Patient-specific aortic outlet boundary modeling

The modeling of aortic outlet should reflect the transiency of blood flow and the elasicity of blood vessels. We used the electrical circuit analogous model such as Fig. 2(a) to reflect these blood flow properties of aortic outlet (Vignon-Clementel et al., 2010; Zhang et al., 2014; Mirramezani et al., 2019).

As can be seen, aortic outlet is modeled by serially connecting the proximal resistance Rp to the parallel connection of compliance C and the distal resistance Rd of blood vessel. The blood pressure and flow rate balance equations at electrical circuit analogous model prescribed at the aortic outlet shown in Fig. 2(a) are as follows:

ISSN No. 2321-2705 | DOI: 10.51244/IJRSI | Volume XII Issue XV October 2025 | Special Issue on Public Health

$$\begin{cases} R_p Q + P_C = P \\ R_p Q + R_d Q_d = P \\ Q_C + Q_d = Q \\ Q_C = C \dfrac{dP_C}{dt} \end{cases} \quad (1)$$

where Q and P are proximal flow rate and pressure, respectly, QC is flow rate accumulated by compliance of blood vessel and PC is pressure drop due to the compliance of blood vessel, Qd is distal flow rate.

Assuming that the simulation is started at t=0, proximal pressure P(t) at time t is expressed from the above systems of ordinary differential equations, Eq. 1 as follows:

$$P(t) = \left[P(0) - R_p Q(0)\right] e^{-\frac{t}{R_d C}} + R_p Q(t) + \int_0^t \frac{e^{-\frac{t-\tilde{t}}{R_d C}}}{C} Q(\tilde{t}) d\tilde{t} \quad (2)$$

Eq. 2 means that blood pressure at time t is related to the flow history between time 0 and the current time t.

2.2.2. Patient-specific coronary outlet boundary modeling

The coronary outlet is modeled by coupling of coronary arterial resistance Ra, coronary arterial compliance Ca, microcirculatory resistance Ram, myocardial compliance Cim, coronary venous resistance Rv and ventricular pressure Pim as shown in Fig. 2(b) (Mirramezani et al., 2019).

In this case coronary venous compliance and coronary venous microcirculatory resistance omitted from the analogous model because they have little effect on coronary pressures and flow waveforms. The blood pressure and flow rate balance equations at subcircuit of electrical circuit analogous model shown in Fig. 2(b) are as follows:

$$\begin{cases} R_{am} Q_1 + P_{Cim} + P_{im} = P_{Ca} \\ R_{am} Q_1 + R_v Q_{11} = P_{Ca} \\ Q_{11} + Q_{12} = Q_1 \\ Q_{12} = C_{im} \dfrac{dP_{Cim}}{dt} \end{cases} \quad (3)$$

PCa(t) is obtained from the systems of ordinary differential equations, Eq. 3 as follows.

$$P_{Ca}(t) = R_{am} Q_1(t) + \frac{1}{R_v C_{im}} e^{-\frac{t}{R_v C_{im}}} \int e^{\frac{t}{R_v C_{im}}} \left[R_v Q_1(t) - P_{im}(t)\right] dt + P_{im}(t) \quad (4)$$

where the ventricular pressure Pim(t) is expressed by end-diastolic volume of ventricle Vedv and elastance function of ventricle E(t) as follows (Kim et al., 2009):

$$P_{im}(t) = E(t) \cdot \left(V_{edv} - \int_0^t Q(\tilde{t}) d\tilde{t} - V_0 \right) \quad (5)$$

where V0 is calculated by end-systolic volume of ventricle Vesv, systolic pressure Psys and the maximum elastance of ventricle Emax as follows (Kim et al., 2009):

$$V0 = Vesv - 0.9Psys/Emax \quad (6)$$

And the following equations are satisfied from Fig. 2(b).

ISSN No. 2321-2705 | DOI: 10.51244/IJRSI | Volume XII Issue XV October 2025 | Special Issue on Public Health

$$\begin{cases} R_a Q_0 + P_{Ca} = P_0 \\ Q_1 + Q_2 = Q_0 \\ Q_2 = C_a \dfrac{dP_{Ca}}{dt} \end{cases} \tag{7}$$

From the second and third expressions of Eq. 7, we have:

$$\frac{Q_0 - Q_1}{C_a} = \frac{dP_{Ca}}{dt} \tag{8}$$

Sustituting Eq. 4 into Eq. 8, we obtain:

$$\begin{aligned} &\frac{1}{R_v^2 C_{im}^2} e^{-\frac{t}{R_v C_{im}}} \int e^{\frac{t}{R_v C_{im}}} (R_v Q_1 - P_{im}) dt \\ &\quad = R_{am} \frac{dQ_1}{dt} + \frac{dP_{im}}{dt} + \frac{1}{R_v C_{im}} (R_v Q_1 - P_{im}) - \frac{Q_0 - Q_1}{C_a} \end{aligned} \tag{9}$$

Differentiating both sides of Eq. 9 with respect to t, it is expressed as follows:

$$\begin{aligned} &\frac{1}{R_v^2 C_{im}^2} \left(-\frac{1}{R_v C_{im}} \right) e^{-\frac{t}{R_v C_{im}}} \int e^{\frac{t}{R_v C_{im}}} (R_v Q_1 - P_{im}) dt + \frac{1}{R_v^2 C_{im}^2} e^{-\frac{t}{R_v C_{im}}} e^{\frac{t}{R_v C_{im}}} (R_v Q_1 - P_{im}) \\ &\quad = R_{am} \frac{d^2 Q_1}{dt^2} + \frac{d^2 P_{im}}{dt^2} + \frac{1}{R_v C_{im}} \left(R_v \frac{dQ_1}{dt} - \frac{dP_{im}}{dt} \right) - \frac{1}{C_a} \left(\frac{dQ_0}{dt} - \frac{dQ_1}{dt} \right) \end{aligned} \tag{10}$$

Substituting Eq. 9 into Eq. 10, we obtain:

$$\begin{aligned} &R_{am} \frac{d^2 Q_1}{dt^2} + \left(\frac{1}{C_{im}} + \frac{1}{C_a} + \frac{R_{am}}{R_v C_{im}} \right) \frac{dQ_1}{dt} + \frac{Q_1}{R_v C_{im} C_a} \\ &\quad = \frac{Q_0}{R_v C_{im} C_a} + \frac{1}{C_a} \frac{dQ_0}{dt} - \frac{d^2 P_{im}}{dt^2} \end{aligned} \tag{11}$$

Eq. 11 is a nonhomogeneous second order ordinary differential equation, which can be expressed as follows:

$$\frac{d^2 Q_1}{dt^2} + A \frac{dQ_1}{dt} + B Q_1 = f(t) \tag{12}$$

where

$$A=\frac{1}{R_{am}}\left(\frac{1}{C_{im}}+\frac{1}{C_a}+\frac{R_{am}}{R_vC_{im}}\right),$$

$$B=\frac{1}{R_{am}}\frac{1}{R_vC_{im}C_a},$$

$$f=\frac{1}{R_{am}}\left(\frac{Q_0}{R_vC_{im}C_a}+\frac{1}{C_a}\frac{dQ_0}{dt}-\frac{d^2P_{im}}{dt^2}\right)$$

Obtaining Q1 from Eq. 12 and considering Eq. 4, the pressure P0(t) at the coronary outlet is obtained by the first equation of Eq. 7 as follows:

$$P0(t)=RaQ0(t)+PCa(t) \quad (13)$$

where Q0(t) is flow rate at the coronary outlet.

Optimization of parameter values

In order to extract the aortic and coronary outlet pressure waveforms from Eq. 2 and Eq. 13, we must know the compliance C, distal resistance Rd and proximal resistance Rp of aortic blood vessel and the coronary arterial resistance Ra, coronary arterial compliance Ca, coronary arterial microcirculatory resistance Ram, myocardial compliance Cim and coronary venous resistance Rv.

Considering the properties of blood vessels, we assume that these parameters are in the following range.

104Pa•s/m3<Rd, Rp, Ra, Ram, Rv<1011Pa•s/m3

10-10m3/Pa<C, Ca, Cim<10-6m3/Pa

And max-systolic pressure Pmax and the time of the peak systolic tmax, min-diastolic pressure Pmin and the time of the minimum diastolic tmin can be obtained by clinical examination.

Hence, we can set up the following optimization problems:

$$\begin{cases}10^4<R_d,R_p<10^{11}\\10^{-10}<C<10^{-6}\\\min F=\left[P(t_{\max})-P_{\max}\right]^2+\left[P(t_{\min})-P_{\min}\right]^2\end{cases} \quad (14)$$

$$\begin{cases}10^4<R_a,R_{am},R_v<10^{11}\\10^{-10}<C_a,C_{im}<10^{-6}\\\min F_0=\left[P_0(t_{\max})-P_{\max}\right]^2+\left[P_0(t_{\min})-0\right]^2\end{cases} \quad (15)$$

Thus, the parameters are optimized such that the maximum systolic pressure at the time of the peak systolic and the minimum diastolic pressure at the time of the minimum diastolic obtained by clinical measurements are equal to the values obtained by Eq. 2 and Eq. 13.

The optimization problem such as Eq. 14 and Eq. 15 can be solved using particle swarm optimization (PSO) algorithm. The PSO algorithm is a stochastic global search approach that selects the optimal solution candidates of the search space as “particle swarms” and that each particle in the swarm continues to update its position probabilistically using its optimal information and the optimal information of the swarm at each iteration step, and then approaches the optimal solution. The PSO algorithm is very simple programmable and very efficient because it has a simple arithmetic operation.

ISSN No. 2321-2705 | DOI: 10.51244/IJRSI | Volume XII Issue XV October 2025 | Special Issue on Public Health

The general flowchart of the PSO algorithm is shown in Fig. 3.

The PSO algorithm is compared and evaluated by applying other algorithms such as genetic algorithms to neural network training problems and standard benchmark functions, and it is verified that the computational effort is small and convergence is good. Using such particle swarm optimization (PSO) algorithm, the optimization problems are solved to determine the parameters for the aortic and coronary outlets and thus the blood pressure waveforms at the aortic and coronary outlets can be obtained by Eq. 2 and Eq. 13.

The parameter settings for the detailed example are given below.

Simulation details

By constructing a cardiovascular geometry of a heart disease patient and by setting the aortic inlet blood flow waveform and the coronary outlet blood pressure waveforms by the indices obtained from clinical measurement and the above parameters as boundary conditions, the blood flow simulation analysis is performed by ANSYS Fluent 19.2.

The characteristic indices of blood flow in cardiovascular system are obtained from clinical examination.

The aortic inlet blood flow waveform of patient with heart rate of 75beats/min, cardiac output of 4.32L/min, diastolic pressure of 80mmHg and systolic pressure of 110mmHg, respectively, is like as Fig. 4.

And the aortic and coronary outlet parameters obtained by clinical measurements and the optimization problems Eq. 14 and Eq.15 are listed in Table 1 and Table 2.

According to the above parameters, the blood pressure waveforms at the aortic and coronary outlets obtained from Eq. 2 and Eq. 13 are shown in Fig. 5.

Fig. 5 shows that the maximum systolic pressure and the minimum diastolic pressure are 110mmHg and 80mmHg at the aortic outlet, respectively, which is consistent with the clinical measurements. And the maximum systolic pressure is 110mmHg and the minimum diastolic pressure is about 10mmHg in the coronary outlet, which shows the properties of coronary outlets well.

And blood was approximated as an incompressible Newtonian fluid with density of 1 058 kg/m3 and viscosity of 0.004 1 Pa•s. These values were measured by blood tests. The vascular walls were considered as rigid, inelastic and impermeable.

Blood flow in a cardiovascular system may be regarded as laminar flow because Reynolds number Re is relatively small, but it is more accurate to consider turbulent flow because the vortex is involved in the separation of the cardiovascular system. Hence, the flow model for the blood flow analysis was regarded as the Realizable k-ε turbulent model.

We also used the Semi-Implicit Method for Pressure-Linked Equations Consistent (SIMPLEC) scheme as the pressure-velocity coupling scheme, the Standard scheme for pressure and the Second Order Upwind schemes for momentum, turbulent kinetic energy and turbulent dissipation rate as spatial discretization schemes, and Crank-Nicholson approximation scheme as the time-stepping scheme.

For the initial condition the whole model is initializes using the inlet flow rate at time t=0s.

RESULTS AND DISCUSSION

Setting the above aortic inlet blood flow waveform, aortic outlet blood pressure waveform and coronary outlet blood pressure waveforms as inlet and outlet boundary conditions, we carried out analysis of vascular model as like Fig. 1 by analysis program, ANSYS Fluent 19.2 during two cardiac cycles.

To analyze the effect of mesh number on the simulation results, the analysis was performed by varying mesh number to calculate the mean blood pressure at the aortic inlet and the results are shown in Fig. 6.

ISSN No. 2321-2705 | DOI: 10.51244/IJRSI | Volume XII Issue XV October 2025 | Special Issue on Public Health

As shown in the figure, with the increase of mesh number, the variation of mean aortic pressure gradually decreased, and it was very small, less than 1% since the mesh number was about 500 000. From this mesh independence analysis, the mesh model was composed of 496 617 meshes and 65 225 nodes, and the time step was set to 10-4 s, and transient analysis was performed to obtain blood pressure distribution and blood flow waveforms.

Blood pressure distributions

To verify the accuracy of the simulation, the blood pressure distribution in the vessel wall is analyzed and compared with the results obtained by clinical measurements.

Fig. 7 shows the blood pressure contours of cardiovascular system at the time of peak systole and minimum diastole.

This figure shows the blood pressure drop from the aorta to the coronary artery branches visually, especially in the constrictive branches, a significant blood pressure drop was observed.

The results of the analysis shows that the aortic blood pressure at the time of peak systole and at the time of minimum diastole was 112.77mmHg and 79.12mmHg, respectively, which are in close agreement with the systolic pressure of 110mmHg and diastolic pressure of 80mmHg obtained by clinical measurements. The relative error is 2.55% at the peak systolic pressure and -1.12% at the minimum diastolic pressure, which shows the accuracy of the simulation analysis.

Blood flow waveforms

Blood flow at the vascular outlet is very important to meet the oxygen demand of the cardiac circulation, and therefore, insufficient blood flow is a major cause of the development of blood deficiency. Thus, blood flow rates at each vascular outlet were calculated.

Fig. 8 shows the aortic and coronary outlet blood flow waveforms.

From the figure, the blood flow rate at the coronary arteries is large in the diastole and small in the systole because the intramyocardial pressure caused by the ventricular pressure is high in the systole.

Table 3 shows the mean flow rate to every branch of coronaty artery.

From the table, the flow rates to RCA_1 and RCA_5 are much lower than to the others because the vascular diameter at their proximal part became narrow by stenosis. And the flow rate to the right coronary artery is 2.606 mL/s, the flow rate to the left coronary artery is 2.152 mL/s, which yields a total coronary flow of 4.758 mL/s. A typical 3/7 flow split between RCA and LCA is enforced (Sankaran et al., 2012) but the above result shows that the flow rate to the left coronary artery is rather less than that to the right coronary artery, because there is a stenosis with 50% area-reduction in proximal of the main left coronary artery. If there is no stenosis in proximal of the main left coronary artery, the flow rate will be markedly incresed to the left coronary artery and the typical flow split between RCA and LCA will be satisfied.

And from the simulation results, the flow rate to the aortic outlet is 50.1 mL/s, and consequently cardiac output computed from simulation analysis is 4.11L/min, which nearly coincides with 4.32L/min as the cardiac output obteined by clinical examination

Finally, it shows that the boundary modeling method and the simulartion analysis method are well-suited to the patient-specific characteristics.

Setting the boundary conditions by above inlet and outlet boundary modeling method for cardiovascular models of 30 patients with cardiovascular disease, we analyzed blood flow in cardiovascular system by ANSYS Fluent 19.2 and compared with clinical measurements. The comparison results are shown in Table 4.

Comparing the simulation analysis results and the clinical measurements, Table 4 shows that the relative error

of systolic pressure, diastolic pressure and cardiac output are -3.94~4.42%, -2.71~4.43% and -4.76~4.8% respectively, which verifys the accuracy of boundary modeling and simulation analysis method.

CONCLUSION

In this paper, we suggested a method to extract patient-specific aortic and coronary outlet blood pressure waveforms from the electrical circuit analogous models by solving the analogous circuit equations, and set those waveforms as boundary conditions to analyze blood flow in the cardiovascular system by using ANSYS Fluent 19.2. Through the study of the simulation analysis results of several patient-specific cardiovascular models we confirmed the accuracy of the electrical circuit analogous models for the aortic and coronary outlets, and the validity of the optimization for choosing parameters and the computational fluid dynamics blood fluid flow simulation method. Our developing simulation system includes the optimizing process for choosing optimal parameters, the discretization process of the basic equations, the modeling process of blood flow and the solving process discretization schemes for simulating and analyzing blood flow, so it is not easy to verify the correctness of every step in process of developing. Hence, we suggested the comparison with the analysis results by ANSYS Fluent 19.2 as a solution to verify the accuracy of analysis results by our simulation system. In order to set boundary conditions for simulation analysis by ANSYS Fluent 19.2, we extracted outlet blood pressure waveforms from the electrical circuit analogous models modeled by our simulation system. And we carried out blood flow simulation analysis of patient-specific three-dimensional vascular models made by our simulation system by using ANSYS Fluent 19.2 and compared that result with clinical measurements. The comparison between the results from ANSYS Fluent 19.2 and the clinical measurements shows that the relative errors of the clinical indices such as blood pressure and cardiac output are all less than ±5%. These study results verify the correctness of blood pressure waveform extraction method and blood flow simulation method by using ANSYS Fluent 19.2 and demonstrate the validity of analysis results from ANSYS Fluent 19.2 as comparative proposition. And those made accelerate our simulation system development by verifying the correctness of blood simulation results from our simulation system. The boundary setting method and simulation method suggested in this paper can be applied effectively to CFD analysis of blood flow in vascular.

ACKNOWLEDGMENT

The authors are grateful to Dr. Il-Guk Jo for his valuable suggestions during the completion of this paper.

Funding information

None

Authors' contribution

Ji-Song Jong conceived the study concept and design, participated in analysis and interpretation, and drafted and revised the manuscript.

Ji-Song Thak studied the boundary condition modeling method.

Sung-Ri Kim performed literature study and data analysis.

Hyon-Chol Choe participated in CFD analysis of blood flow.

Kuk-Chol Song participated in clinical data acquisition and analysis.

All authors read and approved the final manuscript.

Conflict of interests

The authors declare that they have no conflict of interest.

Ethical approval

The conducted research is not related to either human or animal use.

Data availability statement

The data that support the findings of this study are available from [third party name] but restrictions apply to the availability of these data, which were used under license for the current study, and so are not publicly available. Data are however available from the authors upon reasonable request and with permission of [third party name].

REFERENCES

1. Aboelkassem, Y., Virag, Z., 2019. A hybrid Windkessel-Womersley model for blood flow in arteries. Journal of Theoretical Biology 462, 499-513.
2. Ballarin, F., Faggiano, E., Manzoni, A., Quarteroni, A., Rozza, G., Ippolito, S., Antona, C., Scorofani, R., 2017. Numerical modeling of hemodynamics scenarios of patient-specific coronary artery bypass grafts. Biomech Model Mechanobiol 16, 1373-1399.
3. Bertolotti, C., Deplano, V., 1999. Three-dimensional numerical simulations of flow through a stenosed a coronary bypass. Journal of Biomechanics 33, 1011-1022.
4. Fan, T.T., Lu, Y., Gao, Y., Meng, J., Tan, W.C., Huo, Y.L., Kassab, G.S., 2016. Hemodynamics of left internal mammary artery bypass graft: Effect of anastomotic geometry, coronary artery stenosis, and postoperative time. Journal of Biomechanics http://dx.doi.org/10.1016/j.jbiomech.2016.01.031.
5. Fayssal, I.A., Moukalled, F., Alam, S., Isma'eel, H., 2018. An outflow boundary condition model for noninvasive prediction of fractional flow reserve in diseased coronary arteries. Journal of Biomechanical Engineering 140, 041004-1-13.
6. Hazer, D., Unterhinninghofen, R., Kostrzewa, M., Kauczor, H.U., Dillmann, R., Richter, G.M., 2006. A workflow for computational fluid dynamics simulations using patient-specific aortic models. 24th CADFEM Users' Meeting 2006 International Congress on FEM Technology with 2006 German ANSYS Conference, Germany.
7. Horner, M., Wang, X.S., Pietila, T., George, E., 2016. RSNA 2016 Introduction to computational fluid dynamics from medical images: A step-by-step demonstration (Hands-on) Training Guide. Applied Imaging Science Lab.
8. Jayendiran, R., Nour, B., Ruimi, A., 2018. Computational fluid–structure interaction analysis of blood flow on patient-specific reconstructed aortic anatomy and aneurysm treatment with Dacron graft. Journal of Fluid and Structures 81, 693-711.
9. Kamangar, S., Badruddin, I.A., Govindaraju, K., Nik-Ghazali, N., Badarudin, A., Viswanathan, G.N., Salman Ahmed, N.J., Yunus Khan, T.M., 2017. Patient-specifc 3D hemodynamics modelling of left coronary artery under hyperemic conditions. Med. Biol. Eng. Comput. 55, 1451-1461.
10. Kandail, H.S., Trivedi, S.D., Shaikh, A.C., Bajwa, T.K., O'Hair D.P., Jahangir, A., LaDisa, J.F., 2018. Impact of annular and supra-annular core valve deployment locations on aortic and coronary artery hemodynamics. Journal of the Mechanical Behavior of Biomedical Materials https://doi.org/10.1016/j.jmbbm.2018.06.032.
11. Vignon-Clementel, I.E., Coogan, J.S., Figueroa, C.A., Jansen, K.E., Taylor, C.A., 2010. Patient-specific modeling of blood flow and pressure in human coronary arteries. Annals of Biomedical Engineering 38(10), 3195-3209.
12. Vignon-Clementel, I.E., Figueroa, C.A., LaDisa, J.F., Jansen, K.E., Feinstein, J.A., Taylor, C.A., 2009. On coupling a lumped parameter heart model and a three-dimensional finite element aorta model. Annals of Biomedical Engineering 37, 2153–2169.
13. Ko, T.H., Ting, K., Yeh, H.C., 2007. Numerical investigation on flow fields in partially stenosed artery with complete bypass graft: An in vitro study. International Communications in Heat and Mass Transfer, 34, 713-727.
14. Lan, H.Z., Updegrove, A., Wilson, N.M., Maher, G.D., Shadden, S.C., Marsden, A.L., 2018. A re-engineered software interface and workflow for the open-source SimVascular cardiovascular modeling package. Journal of Biomechanical Engineering 140, 024501-1-11.
15. McGah, P.M., Leotta, D.F., Beach, K.W., Riley, J.J., Aliseda, A., 2011. A Longitudinal Study of Remodeling in a Revised Peripheral Artery Bypass Graft Using 3D Ultrasound Imaging and Computational Hemodynamics. Journal of Biomechanical Engineering 133, 041008-1-10.
16. Mirramezani, M., Diamond, S.L., Litt, H.I., Shadden, S.C., 2019. Reduced order models for transstenotic pressure drop in the coronary arteries. Journal of Biomechanical Engineering 141, 031005-1-11.

17. Owida, A.A., Do, H., Morsi, Y.S., 2012. Numerical analysis of coronary artery bypass grafts: An over view. Computer Methods and Programs in Biomedicine 108, 689-705.
18. Politis, A.K., Stavropoulos, G.P., Christolis, M.N., Panagopoulos, F.G., Vlachos, N.S., Markatos, N.C., 2007. Numerical modeling of simulated blood flow in idealized composite arterial coronary grafts: Steady state simulations. Journal of Biomechanics 40, 1125-1136.
19. Sankaran, S., Moghadam, M.E., Kahn, A.M., Tseng, E.E., Guccione, J.M., Marsden, A.L., 2012. Patient-specific multiscale modeling of blood flow for coronary artery bypass graft surgery. Annals of Biomedical Engineering 40(10), 2228-2242.
20. Schiavazzi, D.E., Hsia, T.Y., Marsden, A.L., 2016. On a sparse pressure-flow rate condensation of rigid circulation models. Journal of Biomechanics 49, 2174-2186.
21. Segalova, P.A., Venkateswara Rao, K.T., Zarins, C.K., Taylor, C.A., 2012. Computational modeling of shear-based hemolysis caused by renal obstruction. Journal of Biomechanical Engineering 134, 021003-1-7.
22. Schiavazzi, D.E., Kahn, A.M., Marsden, A.L., 2020. The effects of clinically-derived parametric data uncertainty in patient-specific coronary simulations with deformable walls. arXiv:1908.07522v2 [physics.med-ph].
23. Shaik, E., Hoffmann, K.A., Dietiker, J.F., 2008. Numerical simulations of pulsatile non-Newtonian flow in an end-to-side anastomosis model. Simulation Modelling Practice and Theory 16, 1123-1135.
24. Updegrove, A., Wilson, N.M., Merkow, J., Lan, H.Z., Marsden, A.L., Shadden, S.C., 2017. SimVascular: An open source pipeline for cardiovascular simulation. Annals of Biomedical Engineering 45(3), 525-541.
25. Vignon-Clementel, I.E., Figueroa, C.A., Jansen, K.E., Taylor, C.A., 2010. Outflow boundary conditions for 3D simulations of non-periodic blood flow and pressure fields in deformable arteries. Computer Methods in Biomechanics and Biomedical Engineering 13(5), 625-640.
26. Wang, W., Wang, F., 2014. Numerical simulation of coronary artery bypass graft with an assistant graft. Chinese Journals of Biomedical Engineering 23(1), 38-46.
27. Zambrano, B.A., McLean, N.A., Zhao, X.D., Tan, J.L., Zhong, L., Figueroa, C.A., Laa, L.C., Baek, S.I, 2017. Image-based computational assessment of vascular wall mechanics and hemodynamics in pulmonary arterial hypertension patients. Journal of Biomechanics https://doi.org/10.1016/j.jbiomech.2017.12.022.
28. Zhang, J.M., Zhong, L., Su, B., Wan, M., Yap, J.S., Tham, J.P.L., Chua, L.P., Ghista, D.N., Tan, R.S., 2014. Perspective on CFD studies of coronary artery disease lesions and hemodynamics: A review. International Journal for Numerical Methods in Biomedical Engineering 30, 659-680.
29. Zhao, X., Liu, Y.J., Li, L.L., Wang, W.X., Xie, J.S., Zhao, Z., 2016. Hemodynamics of the string phenomenon in the internal thoracic artery grafted to the left anterior descending artery with moderate stenosis. Journal of Biomechanics 49, 983-991.
30. Zhu, F.P., Karunanithi, K., Qian, Y., Mao, Y., Xu, B., Gu, Y.X., Zhu, W., Chen, L., Wang, Y., Pan, H.W., Liao, Y.J., Morgan, M., 2015. Assessing surgical treatment outcome following superficial temporal artery to middle cerebral artery bypass based on computational haemodynamic analysis. Journal of Biomechanics 48, 4053-4058.

ISSN No. 2321-2705 | DOI: 10.51244/IJRSI | Volume XII Issue XV October 2025 | Special Issue on Public Health

Table 1. The aortic outlet parameters.

$R_p(10^7 Pa \cdot s/m^3)$	$C(10^{-7} m^3/Pa)$	$R_d(10^9 Pa \cdot s/m^3)$
1.626	9.35	3.87

Table 2. The coronary outlet parameters.

Branch	$R_a(10^7 Pa \cdot s/m^3)$	$C_a(10^{-9} m^3/Pa)$	$R_{am}(10^6 Pa \cdot s/m^3)$	$C_{im}(10^{-8} m^3/Pa)$	$R_v(10^5 Pa \cdot s/m^3)$
RCA_1	6.48	7.36	2.73	6.58	1.4
RCA_2	8.23	5.89	4.36	4.75	2.67
RCA_3	8.23	5.89	4.36	4.75	2.67
RCA_4	8.23	5.89	4.36	4.75	2.67
RCA_5	6.48	7.36	2.73	6.58	1.4
LCA_1	4.23	2.98	4.82	1.76	1.9
LCA_2	2.65	4.32	2.87	5.67	3.7
LCA_3	5.46	5.64	3.52	3.98	4.78
LCA_4	5.46	5.64	3.52	3.98	4.78
LCA_5	3.23	6.07	3.45	9.73	6.07
LCA_6	3.23	6.07	3.45	9.73	6.07

Table 3. The coronary outlet blood flow rate.

Branch	Blood flow rate (mL/s)	Branch	Blood flow rate (mL/s)
RCA_1	0.058	LCA_1	0.411
RCA_2	0.994	LCA_2	0.556
RCA_3	0.572	LCA_3	0.319
RCA_4	0.911	LCA_4	0.594
RCA_5	0.071	LCA_5	0.154
		LCA_6	0.118
RCA	2.606	LCA	2.152

Table 4. Comparison between simulation results and clinical measurements.

Model	Systolic pressure (mmHg)			Diastolic pressure (mmHg)			Cardiac output (mL)		
	Simulation result	Clinical data	Relative error (%)	Simulation result	Clinical data	Relative error (%)	Simulation result	Clinical data	Relative error (%)
1	114.3	110	3.91	72.3	70	3.29	4.24	4.42	-4.1

ISSN No. 2321-2705 | DOI: 10.51244/IJRSI | Volume XII Issue XV October 2025 | Special Issue on Public Health

2	103.4	100	3.4	61.5	60	2.5	4.37	4.22	3.36
3	115.7	120	-3.58	83.4	80	4.25	3.6	3.48	3.37
4	113.2	110	2.91	68.5	70	-2.14	3.68	3.82	-3.6
5	119.5	115	3.91	69.3	70	-1	3.86	3.94	-2.05
6	138.2	135	2.37	82.6	80	3.25	4.57	4.47	2.46
7	96.4	100	-3.6	61.9	60	3.17	3.72	3.62	2.54
8	106.3	110	-3.36	72.8	70	4	4.1	4.05	1.07
9	159.3	155	2.77	98.3	100	-1.7	4.94	4.75	3.86
10	131.2	135	-2.81	82.7	85	-2.71	4.5	4.39	2.5
11	134.5	130	3.46	88.4	90	-1.78	4.02	4.15	-3.26
12	144.2	140	3	82.1	80	2.63	4.32	4.2	2.92
13	127.8	130	-1.69	83.5	80	4.38	4.22	4.03	4.60
14	118.2	120	-1.5	78.4	80	-2	3.83	3.67	4.19
15	147.2	150	-1.87	88.7	90	-1.44	4.22	4.06	4.10
16	112.8	110	2.55	79.1	80	-1.12	4.11	4.32	-4.76
17	141.2	140	0.86	90.7	90	0.78	4.77	4.87	-2.13
18	149.3	150	-0.47	81.5	80	1.88	4.02	3.86	4.04
19	153.5	150	2.33	88.9	90	-1.22	4.76	4.61	3.39
20	138.4	140	-1.14	89.1	90	-1.0	4.63	4.42	4.8
21	132.1	130	1.62	81.6	80	2	4.32	4.2	2.93
22	164.8	160	3	93.2	90	3.56	3.84	3.67	4.63
23	125.3	120	4.42	79.2	80	-1	3.82	3.7	3.15
24	153.7	160	-3.94	102.4	100	2.4	3.87	3.74	3.42
25	115.3	120	-3.92	73.1	70	4.43	3.95	4.06	-2.60
26	136.7	140	-2.36	93.4	90	3.78	4.7	4.49	4.61
27	143.2	140	2.29	81.3	80	1.6	3.85	3.94	-2.20
28	117.9	120	-1.75	69.2	70	-1.14	4.05	3.89	4.04
29	124.6	120	3.83	79.4	80	-0.75	3.82	3.65	4.69
30	153.8	150	2.53	81.5	80	1.88	3.83	3.94	-2.80

Figure Legends

Figure 1: Patient-specific three-dimensional geometry of the cardiovascular system.

ISSN No. 2321-2705 | DOI: 10.51244/IJRSI | Volume XII Issue XV October 2025 | Special Issue on Public Health

Figure 2: Electrical circuit analogous model prescribed at the aortic and coronary outlet: (a) aortic outlet (b) coronary outelt.

Figure 3: The general flowchart of the PSO algorithm.

Figure 4: The aortic inlet blood flow waveform.

Figure 5: The aortic and coronary outlet pressure waveforms: (a) aortic outlet (b) LCA_1; (c) LCA_2; (d) LCA_3 and LCA_4; (e) LCA_5 and LCA_6; (f) RCA_1 and RCA_5; (g) RCA_2, RCA_3 and RCA_4.

Figure 6: Grid independence analysis.

Figure 7: Blood pressure contour of cardiovascular system: (a) at the time point of peak systole; (b) at the time point of minimum diastole.

Figure 8: The aortic and coronary outlet blood flow waveforms: (a) aortic outlet; (b) LCA_1; (c) LCA_2; (d) LCA_3; (e) LCA_4; (f) LCA_5; (g) LCA_6; (h) RCA_1; (i) RCA_2; (j) RCA_3; (k) RCA_4; (l) RCA_5.

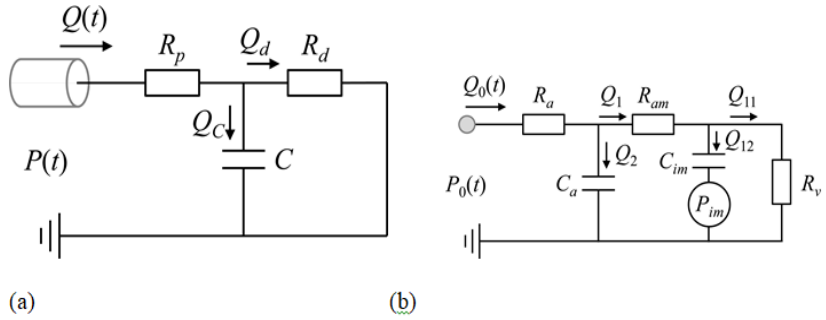

Figure 2

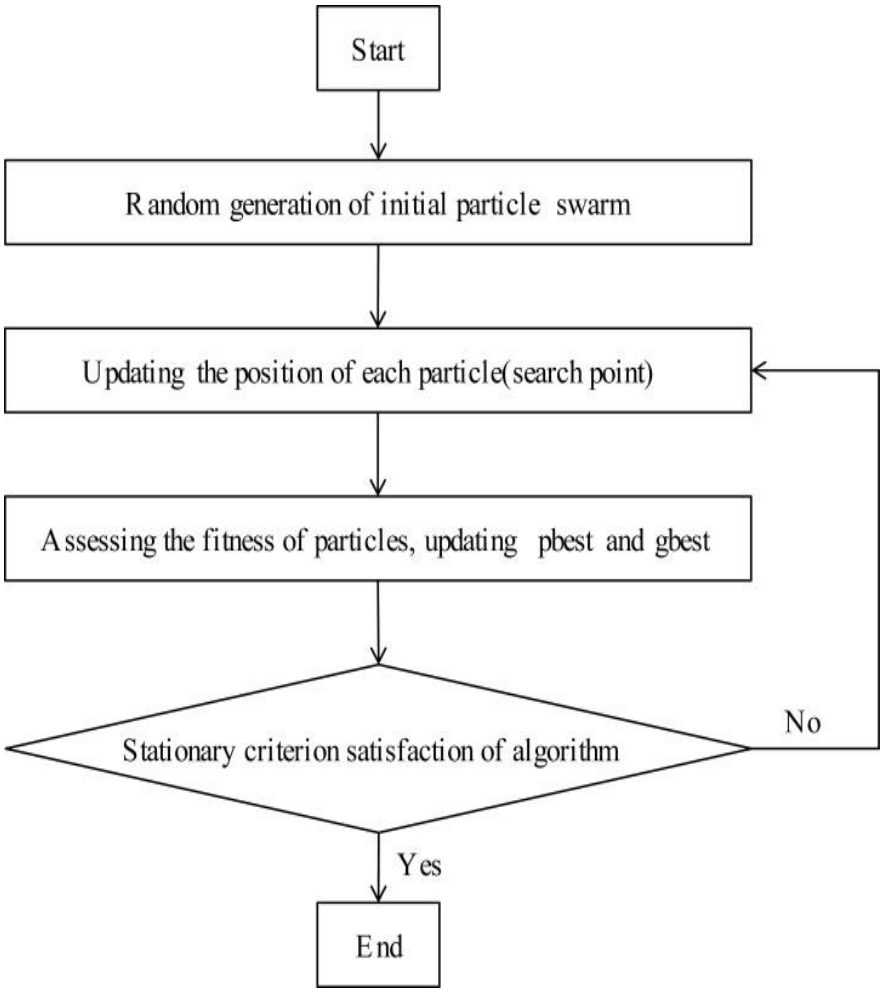

Figure 3

ISSN No. 2321-2705 | DOI: 10.51244/IJRSI | Volume XII Issue XV October 2025 | Special Issue on Public Health

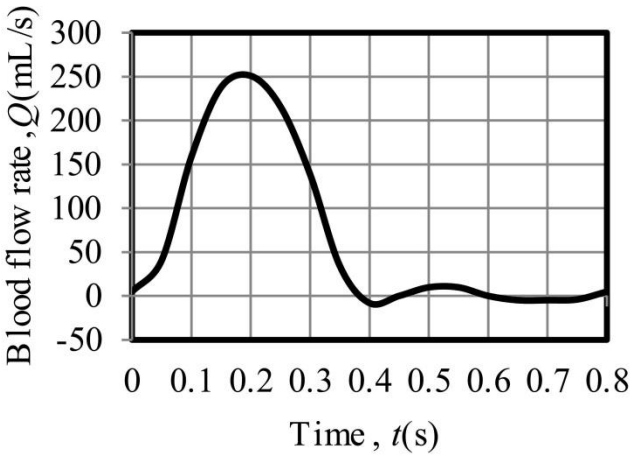

Figure 4

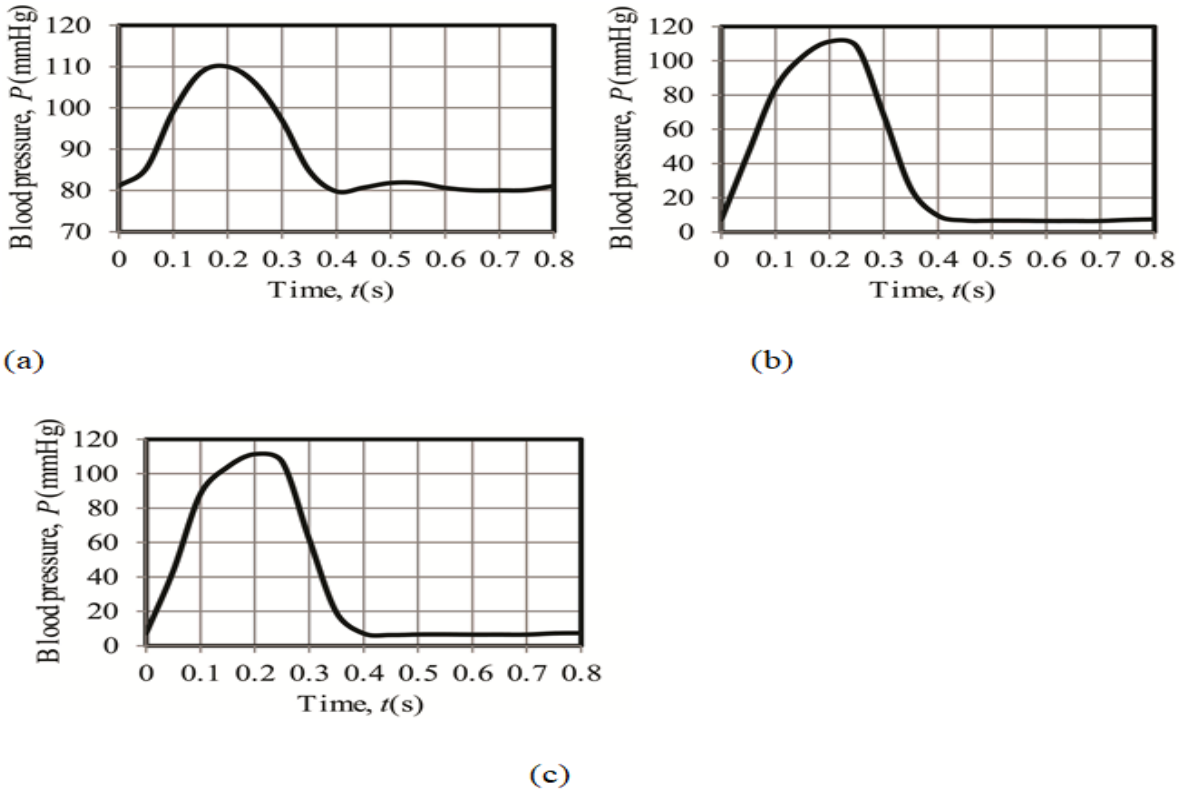

Figure 5

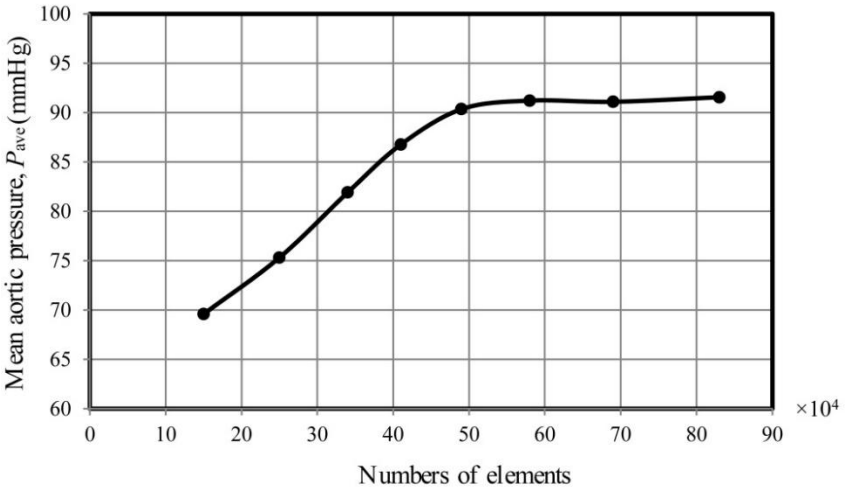

Figure 6

ISSN No. 2321-2705 | DOI: 10.51244/IJRSI | Volume XII Issue XV October 2025 | Special Issue on Public Health

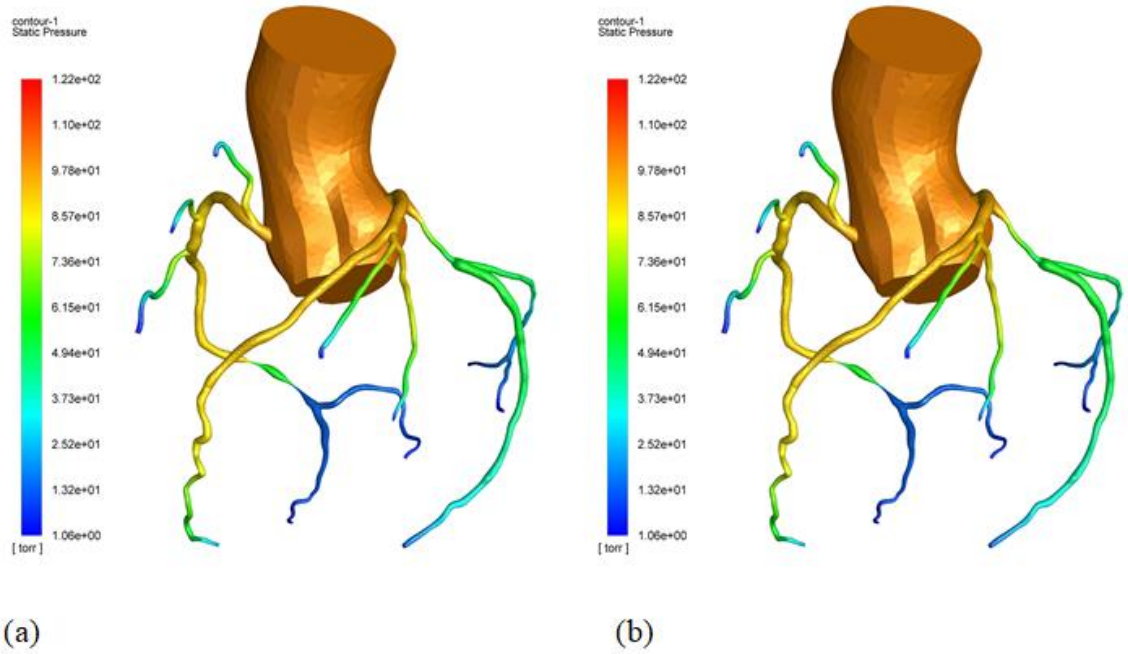

(a) (b)

Figure 7

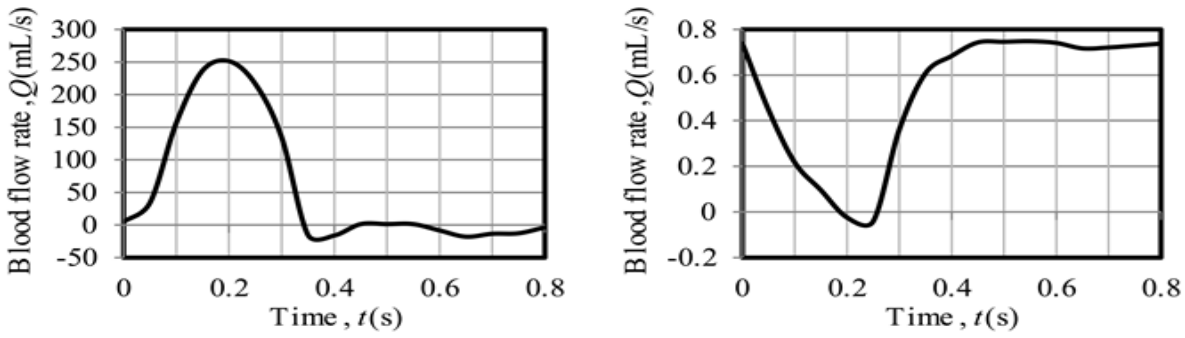

(a) (b)

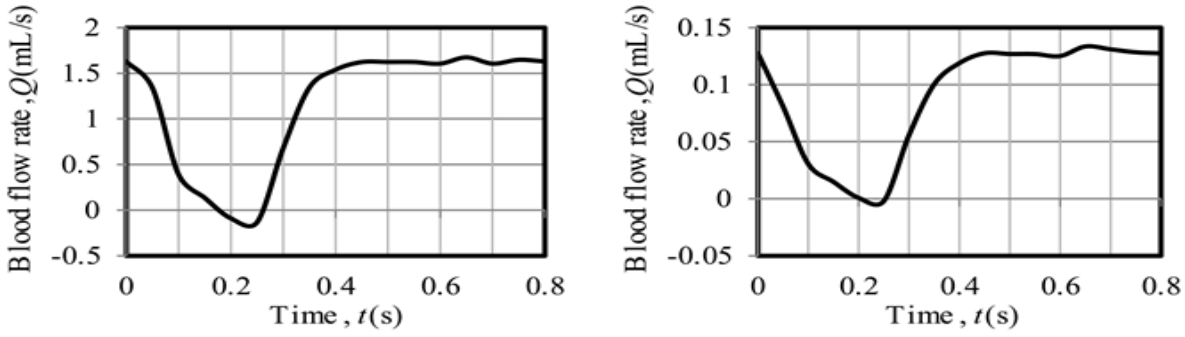

(k) (l)

Figure 8